



Deposited via The University of York.

White Rose Research Online URL for this paper:

<https://eprints.whiterose.ac.uk/id/eprint/123812/>

Version: Accepted Version

Article:

Simmons, Thomas J, Frandsen, Kristian E H, Ciano, Luisa et al. (2017) Structural and electronic determinants of lytic polysaccharide monooxygenase reactivity on polysaccharide substrates. Nature Communications. 1064 (2017). ISSN: 2041-1723

<https://doi.org/10.1038/s41467-017-01247-3>

Reuse

This article is distributed under the terms of the Creative Commons Attribution (CC BY) licence. This licence allows you to distribute, remix, tweak, and build upon the work, even commercially, as long as you credit the authors for the original work. More information and the full terms of the licence here:

<https://creativecommons.org/licenses/>

Takedown

If you consider content in White Rose Research Online to be in breach of UK law, please notify us by emailing eprints@whiterose.ac.uk including the URL of the record and the reason for the withdrawal request.

1 Structural and electronic determinants of lytic polysaccharide
2 monooxygenase reactivity on polysaccharide substrates

3 Simmons TJ^{1*}, Frandsen KEH^{2*}, Ciano L³, Tryfona T¹, Lenfant N^{4,5}, Poulsen JC², Wilson
4 LFL¹, Tandrup T², Tovborg M⁶, Schnorr K⁶, Johansen KS⁷, Henrissat B^{4,5,8}, Walton PH³, Lo
5 Leggio L² & Dupree P¹.

- 6 1. Department of Biochemistry, University of Cambridge, Cambridge, UK.
7 2. Department of Chemistry, University of Copenhagen, Copenhagen, Denmark.
8 3. Department of Chemistry, University of York, York, UK.
9 4. Architecture et Fonction des Macromolécules Biologiques (AFMB), CNRS, Aix-Marseille
10 Université, Marseille, France.
11 5. Institut National de la Recherche Agronomique (INRA), AFMB, Marseille, France.
12 6. Novozymes A/S, Bagsvaerd, Denmark.
13 7. Department of Geoscience and Natural Resources Management, Copenhagen University,
14 Frederiksberg, Denmark
15 8. Department of Biological Sciences, King Abdulaziz University, Jeddah, Saudi Arabia.

16 *These authors contributed equally to this work

17 Correspondence and requests for material should be sent to L.L.L. (email: leila@chem.ku.dk) or
18 P.D. (email: pd101@cam.ac.uk)

19 **Abstract**

20 Lytic polysaccharide monooxygenases (LPMOs) are industrially important copper-
21 dependent enzymes that oxidatively cleave polysaccharides. We studied two closely
22 related AA9-family LPMOs from *Lentinus similis* (*LsAA9A*) and *Collariella virescens*
23 (*CvAA9A*). *LsAA9A* and *CvAA9A* cleave a range of polysaccharides, including cellulose,
24 xyloglucan, mixed-linkage glucan, and glucomannan. *LsAA9A* additionally cleaves isolated
25 xylan substrates, the first LPMO to show such activity. Insights into the determinants of
26 specificity come from the structures of *CvAA9A* and of *LsAA9A* bound to cellulosic and
27 non-cellulosic oligosaccharides. EPR spectra further reveal differences in copper co-
28 ordination on binding of xylan compared to glucans. *LsAA9A* activity is notably less
29 sensitive to reducing agent potential on xylan when compared to other substrates,
30 suggesting a different mechanistic pathway for the cleavage of xylan. These data show
31 that AA9 LPMOs can display different apparent substrate specificities dependent upon
32 both productive protein:carbohydrate interactions across a binding surface and also
33 electronic considerations at the copper active site.

35 The need for sustainable sources of energy and materials has spurred significant research
36 efforts toward a greater understanding of the biological catabolism of lignocellulose, the
37 world's most abundant source of renewable material and bioenergy^{1,2}. The inherent
38 recalcitrance of lignocellulose, however, is one of the major barriers to the utilization of
39 biomass. This recalcitrance is a consequence of both the heterogeneous composition and
40 the often semi-crystalline association of the polymers^{3,4}. In addressing the problem of
41 recalcitrance, multiple potential means have been proposed and assessed, including
42 chemical, mechanical and enzymatic methods. Advances in enzyme cocktail formulations
43 that accelerate the saccharification step of cell wall breakdown⁵, in particular the inclusion
44 of the lytic polysaccharide mono-oxygenases (LPMOs)⁶, are helping cellulosic-ethanol
45 biorefineries move toward both commercial and environmental viability.

46 LPMOs are O₂ and reducing-agent dependent copper metalloenzymes now classified as
47 Auxiliary Activity families AA9–AA11 and AA13⁷⁻¹¹. Extensive spectroscopic and structural
48 studies on LPMOs have shown that the enzyme's active site contains a single copper ion,
49 which is coordinated by the amino terminus nitrogen atom, by a side chain nitrogen atom
50 of the N-terminal histidine, and by the side chain nitrogen atom of an additional histidine, in
51 a structural motif known as the histidine brace¹². What is distinctive about LPMOs is that
52 they oxidatively rather than hydrolytically cleave polysaccharides producing saccharides
53 with oxidized ends¹³. LPMOs augment the action of other polysaccharide-degrading
54 enzymes, and accordingly much research attention is devoted to a greater understanding
55 of the enzymatic mechanism and the range of LPMO saccharide substrates.

56 It was first shown that LPMOs could boost the action of cellulases on cellulose and chitin¹⁴⁻
57 ¹⁶, but LPMOs are now known to act on several crystalline substrates such as chitin,
58 cellulose and retrograded starch^{10-12,17}. Later, enzymes with activity against non-crystalline
59 and oligomeric structures were identified^{18,19}. Furthermore, fungal AA9 LPMOs have been
60 shown to be active on soluble substrates such as xyloglucan, mixed-linkage glucan and
61 glucomannan¹⁹⁻²² and on cellulose-bound xylan²³. Conspicuously, an LPMO active on
62 isolated xylan has not been reported. This range of reported substrates however will likely
63 grow. The large number and sequence diversity of LPMOs that individual fungi maintain²⁴,

64 and their disparate expression profiles when the fungi are grown on different
65 polysaccharide substrates^{25,26}, signal that AA9 LPMOs do have distinct, and functionally
66 significant, polysaccharide substrate specificities, although some evolutionary diversity of
67 LPMOs likely arises through their use of different reducing systems^{27,28}.

68 The root causes of LPMO substrate specificity remain poorly understood. This is because
69 LPMO chemistry is a subtle and complex combination of structural and electronic factors,
70 both of which must be taken into account when developing an understanding of the
71 mechanism of action²⁹. The structure-function relationship of substrate specificity and
72 regiospecificity has been recently reviewed^{30,31}. Insight into LPMO:substrate binding can
73 be gained from the structures of LPMOs³⁰ and combined structural and spectroscopic
74 studies of LPMOs in contact with substrate. Recent ITC, NMR and docking studies of an
75 AA9 LPMO from *Neurospora crassa* in contact with oligosaccharides revealed that more
76 extended substrates had significantly higher binding affinities. This is in accord with a
77 multi-point interaction of the substrate with the LPMO surface where the surface loops in
78 some LPMOs remote from the active site enhance binding affinity²¹. The study also
79 showed that a single Cell₆ chain likely spans the copper active site from the -3 to +3 or -2
80 to +4 subsites (subdivisions of the binding cleft numbered relative to the site of
81 cleavage³²), in which the L3 loop (important for interactions with the +3/+4 subsites) and
82 the LC loop (important for binding to approximately -4 subsite) lie at somewhat extended
83 distances from the copper active site. Detailed insight into an AA9 LPMO-substrate
84 interaction came from the first crystal structures of LPMO:oligosaccharide complexes:
85 *Lentinus similis* AA9A (*LsAA9A*) bound to cellohexaose (Cell₆) and Cell₃³³. Cell₆ was
86 shown to bind at subsites -4 to +2 via interactions with aromatic residues, the N-terminal
87 His and a conserved Tyr as well as a number of hydrogen-bonds with other residues in a
88 contoured binding surface on the LPMO. The +2 glucosyl residue exhibits a set of well-
89 defined hydrogen-bonding interactions with amino-acid side chains (Asn28, His66 and
90 Asn67) essentially locking this residue into a fixed position with respect to the active site.

91 Electronic factors around the active site also play a key role in determining reactive
92 mechanism. Changes in the electronic structure of the copper ion, an important factor in
93 the ability of the copper ion to activate O₂, occur upon substrate binding to *LsAA9A*³³.
94 Furthermore, in an illustration of the complexity of substrate-LPMO interaction and the

95 subtle interplay of electronic and structural factors, Cell₆ is bound synergistically with an
96 exogenous ligand on the copper ion. It is likely that the oxidative mechanism adopted by
97 LPMOs can proceed via one or more of several different routes³⁴, the determinants of
98 which depend to varying extents on the substrate, the reducing agent reducing potential
99 and the positioning of the substrate on the LPMO surface. For instance, the means by
100 which electrons are donated to the LPMO active site modulate the apparent range of
101 reactivity^{28,35}.

102 The detailed molecular and electronic insights of the LPMO-substrate interaction afforded
103 by *combined* biochemical, X-ray diffraction and EPR spectroscopic studies can
104 significantly enhance our understanding of LPMO reactivity. We report herein a study into
105 the principal structural and electronic factors of the reactivity of two AA9 LPMOs with a
106 range of substrates. Through X-ray crystal structures studies of *LsAA9A* with bound
107 substrates we illustrate how binding cleft interactions dictate the site of polysaccharide
108 attack. Through comparison with the *CvAA9A* structure, also determined here, we suggest
109 some structural determinants of specificity for the two enzymes. *LsAA9A* is active on
110 isolated xylan, but this activity is associated with a distinct low sensitivity to reducing agent
111 potential and a different copper co-ordination at the active site, which together reveal an
112 alternative mechanistic pathway for LPMO action on this substrate. These data show how
113 AA9 LPMO substrate cleavage is dependent upon both productive protein:carbohydrate
114 interactions across a binding surface and also electronic considerations at the active site.

115 **Results**

116 ***CvAA9A* is an additional AA9 LPMO active on cello-oligosaccharides**

117 To help understand the basis of AA9 substrate specificity, we searched for enzymes
118 related to *LsAA9A* which might also cleave soluble oligosaccharides. Because LPMOs
119 exhibit high variability in their C-termini, we performed a large-scale alignment of LPMO
120 protein sequences using their N-terminal portion³⁶. We selected 98 AA9 sequences that
121 were highly similar in their N-terminal half to *LsAA9A* and 326 sequences that were highly
122 similar to *TaAA9A* in the same region. *TaAA9A* was used for comparison purposes, since
123 it does not show the ability to cleave soluble oligosaccharides. After adding the sequences

124 of 20 AA9 enzymes studied in the literature, a distance tree was built with the resulting 444
125 AA9 sequences (Fig. 1a, Supplementary Table 1). The tree clearly places *LsAA9A* and
126 *TaAA9A* in distinct clades. From the *LsAA9A* clade, we identified an LPMO from *Collariella*
127 *virescens* (*CvAA9A*; 46% sequence similarity to *LsAA9A*) that lacks some residues
128 observed by Frandsen et al.³³ as being involved in enzyme-substrate interactions
129 (Supplementary Fig. 1). All three of the subsite +2 substrate-binding residues in *LsAA9A*
130 (Asn28, His66 and Asn67) are different in *CvAA9A* (Thr28, Arg67 and Val68)
131 (Supplementary Fig. 1). To study the activity of *CvAA9A*, the enzyme was expressed in
132 *Aspergillus oryzae* and successfully purified from the fermentation broth. (Note that
133 expression in this fungal host preserves the natural side-chain methylation at the N-
134 terminal histidine, in contrast to fungal LPMO expression in *Pichia pastoris* and bacterial
135 systems.) On phosphoric acid-swollen cellulose (PASC), *CvAA9A* produced a range of
136 cello-oligosaccharides (Fig. 1b). The cello-oligosaccharide product profile of *CvAA9A* was
137 similar to that of *LsAA9A* and notably shorter than those produced by *TaAA9A*. Indeed,
138 *CvAA9A* readily degraded Cell₆-2-aminobenzamide (Cell₆-2AB) using a C4-oxidising
139 mechanism to yield Cell₃ and oxidized Cell₃-2AB (Supplementary Fig. 2), like *LsAA9A* but
140 unlike *TaAA9A*³³. Therefore, the distance relationships between the three enzymes, as
141 measured using the N-terminal comparison method above, mirror the similarities in
142 activities of the enzymes.

143 **Position-specific cleavage of a range of hemicelluloses**

144 We next determined whether the *LsAA9A* and *CvAA9A* enzymes are active on a range of
145 β -(1→4)-D-glucan-related polysaccharides (Fig. 2, Table 1). Mixed-linkage glucan (MLG) is
146 a β -D-glucan in which three to four (1→4)-linked residues (Cell₃, Cell₄) are separated by
147 single (1→3) bonds, glucomannan has a backbone randomly composed of β -(1→4)-D-
148 glucosyl and β -(1→4)-D-mannosyl residues, xyloglucan is a β -(1→4)-D-glucan with α -
149 (1→6)-D-xylosyl branches, and xylan is a polymer of β -(1→4)-D-xylosyl residues that is
150 similar to β -(1→4)-D-glucan but lacks C6 groups (Fig. 2b). Both *LsAA9A* and *CvAA9A*
151 showed activity against MLG, glucomannan and xyloglucan, producing a range of
152 oligosaccharide products (Fig. 2a). *LsAA9A* also showed some activity on xylan whereas
153 *CvAA9A* showed no measurable activity on this substrate. No LPMO activity was observed
154 on starch (α -(1→4)-D-glucan), laminarin (β -(1→3)-D-glucan) or chitin (poly β -(1→4)-D-

155 GlcNAc) (Supplementary Fig. 3). Altogether, these activities indicate that both *LsAA9A* and
156 *CvAA9A* enzymes only cleave near β -(1→4)-bonds, and that some variation to the
157 cellulosic β -(1→4)-D-glucan, including substitution, linkage and backbone residue, can be
158 accommodated at or near the site of cleavage by both of the enzymes.

159 To identify precise substrate cleavage sites, we studied the products of both *LsAA9A* and
160 *CvAA9A* cleavage of MLG, glucomannan, xyloglucan and xylan (in the case of *LsAA9A*)
161 polysaccharides by MALDI-ToF MS. Minor double oxidation products were observed,
162 indicating cleavage of these hemicelluloses and PASC using both C1- and C4-oxidising
163 mechanisms (Fig. 3; Supplementary Fig. 4, Table 1). We further investigated the site of
164 attack on these different hemicelluloses using differing protocols. On MLG, we observed in
165 the MALDI data a predominance of DP 4, 7 and 10 oligosaccharides indicating that each
166 enzyme favors cleaving within Cell₄ regions over Cell₃ regions (Fig. 3). The inability of
167 *LsAA9A* and *CvAA9A* to cleave β -Glc-(1→4)- β -Glc-(1→3)- β -Glc-(1→4)-Glc (G4G3G4G),
168 despite their ability to cleave Cell₄ (G4G4G4G) (Supplementary Fig. 5), supports the
169 hypothesis that neither enzyme can cleave at β -(1→3)-bonds and require substantial β -
170 (1→4)-linked regions for cleavage. On glucomannan, we employed High-Performance
171 Anion-Exchange Chromatography (HPAEC) analysis of trifluoroacetic acid (TFA)
172 hydrolysates of digestion products to assess the site of cleavage. Notably, the data
173 indicated that cleavage can occur not only between glucosyl residues, but also with
174 mannose at the +1 or -1 subsite (Supplementary Fig. 6). In order to deduce site of attack
175 on xyloglucan we employed xyloglucan DP14–18 oligosaccharides (Supplementary Fig.
176 7). Inspection of the position of substituted glucose (Glc) in the products indicated that
177 xylosyl substitution of Glc at O-6 was accommodated at the -3, -2, -1, +2 and +3 subsites
178 but unsubstituted Glc was always required at subsite +1. In contrast to the *LsAA9A* and
179 *CvAA9A* products on polysaccharides, *LsAA9A* degraded Xyl₆-2AB to yield two trimers
180 using solely a C4-oxidising mechanism (Supplementary Fig. 8), analogous to cleavage of
181 Cell₆-2AB by both *LsAA9A*³³ and *CvAA9A* (Supplementary Fig. 2).

182 To allow a semi-quantitative determination of the influence of sugar structures on enzyme
183 activity, we probed *LsAA9A* and *CvAA9A* cleavage of the soluble Cell₆, xylohexaose (Xyl₆)
184 and mannohexaose (Man₆) oligosaccharides (Supplementary Fig. 9). The *LsAA9A* activity
185 against Cell₆ was substantially (~100-fold) better than its activity on Xyl₆. Consistent with

186 the absence of activity on glucuronoxylan, CvAA9A activity on Xyl₆ was almost
187 undetectable (~1,000-fold less than Cell₆ activity). Although both enzymes showed activity
188 on glucomannan and can cleave adjacent to mannose, activity was scarcely detectable on
189 Man₆ (~10,000-fold less than Cell₆), indicating that the enzymes require some Glc residues
190 within a mannan backbone for activity.

191 Recent results show dependence of the LPMO action on reductant strength^{28,37}. We found
192 that cleavages of MLG, glucomannan and xyloglucan by LsAA9A were sensitive to
193 reducing agent potential, with ascorbate as reductant yielding much higher amount of
194 product (Fig. 4a). In contrast, cleavage of xylan was not sensitive. We corroborated this
195 finding with oligosaccharides, observing that Xyl₆ was poorly sensitive to reducing agent
196 potential, unlike cleavage of Cell₆ where LsAA9A showed much greater activity with
197 ascorbate than pyrogallol³³ (Fig. 4b).

198 **LsAA9A: and CvAA9A:cello-oligosaccharide structures**

199 To help understand the structural basis of LPMO attack on different substrates, we
200 employed crystallographic analyses. We report here an LsAA9A:Cell₅ complex (Fig. 5 and
201 Supplementary Table 4 and 5) which, owing to a lack of significant substrate contacts to
202 symmetry-related molecules, is a more faithful depiction of the binding conformation of a
203 single oligosaccharide to LsAA9A as compared to the original LsAA9A:Cell₆ structure
204 described by Frandsen et al³³. Tyr203 stacking is still a major interaction in LsAA9A:Cell₅
205 but a new hydrogen bond is seen between O6 and Asp150 at subsite -3, and glycosidic
206 torsion angles are closer to ideal values (Supplementary Table 2). Other interacting
207 residues at the negative subsites are Glu148, Arg159 and Ser77 (Fig. 5; Supplementary
208 Table 3). Like the LsAA9A:Cell₆ structure³³, the main interactions to Cell₅ are a network of
209 hydrogen bonds by Asn28, His66 and Asn67 interacting with O2 and O3 at subsite +2, and
210 the interaction with MeHis1 at subsite +1³⁸.

211 To understand better how protein structure might influence the similarities and differences
212 in CvAA9A and LsAA9A substrate cleavage patterns, the X-ray crystal structure of
213 CvAA9A was solved (Supplementary Fig. 10 and Supplementary Tables 3-5). The Cu-
214 coordinating amino acid residues are MeHis1 and His79 (with equatorial distances to the

215 Cu ranging from 2.0-2.1Å), while a non-coordinating Tyr169 occupies the axial position
216 (2.6-2.8Å). No exogenous ligands are evident within 3.0 Å of the Cu ion indicating that the
217 active site is mostly in a photoreduced Cu(I) state. A “pocket-water” is bound in an H-bond
218 network with the amide-nitrogen and oxygen of Asp76 and MeHis1, respectively. The
219 active site geometry of CvAA9A thus closely resembles that of LsAA9A (Supplementary
220 Fig. 10c). However, there are some amino acid differences in CvAA9A compared to
221 LsAA9A at subsites +2 and -1. Crystals of CvAA9A were soaked with Cell₃ and Cell₆
222 oligosaccharides but this did not result in any catalytically relevant complex.

223 **LsAA9A:hemicellulose oligosaccharide structures**

224 To study the structural determinants of the LsAA9A positional specificity of cleavage, a
225 number of LsAA9A crystal structures in complex with MLG, glucomannan and xylo-
226 oligosaccharides were solved (see Supplementary Tables 2–5 for experimental and
227 crystallographic data and refinement information, hydrogen bonding interactions between
228 enzyme and ligand, and ligand conformations). Soaking experiments with commercially
229 available xyloglucan fragments failed to produce crystallographic complexes, possibly
230 because the substrate oligosaccharides are large and binding likely to be impeded by
231 crystal contacts.

232 *Complexes with MLG tetrasaccharide*

233 LsAA9A crystals were soaked with two different MLG tetrasaccharides, each with a single
234 β-(1→3)-linkage: G4G4G3G and G4G3G4G. Interestingly, the LsAA9A:G4G4G3G
235 complex did not reveal any β-(1→3)-linkages. An apparent Cell₄ substrate appears to be
236 bound from subsite -2 to +2 (Supplementary Fig. 11) giving essentially identical
237 interactions as the -2 to +2 glucosyl residues in the LsAA9A:Cell₅ complex. We interpret
238 this result as the β-(1→4)-glucan (Cell₃) part of the substrate being bound in two
239 overlapping conformations in different asymmetric units from subsites -2 to +1 and -1 to
240 +2, while the β-(1→3)-glucosidic residues are completely disordered in both cases. A
241 structure of LsAA9A crystals soaked with G4G3G4G (not shown) showed very little
242 difference density, which could not be convincingly modelled, further indicating that the

243 enzyme needs at least two consecutive β -(1 \rightarrow 4)-linkages (a Cell₃ unit) for recognition and
244 efficient binding.

245 *Complexes with glucomannan oligosaccharides*

246 *LsAA9A* crystals were soaked with a mixture of glucomannan oligosaccharides. The
247 resulting difference density was well defined clearly showing glycosyl units occupying
248 subsites -3 to $+2$, additional density at -4 and some residual density occupying subsite $+3$
249 (Fig. 6a and 6c). Consistent with the activity data, the structure unequivocally showed a
250 mannosyl unit at the $+1$ subsite, while glucosyl units were clearly observable at -2 , -1 and
251 $+2$ subsites. Moreover the C2 hydroxyl of the mannosyl unit at subsite $+1$ points towards
252 the face of the imidazole side chain of MeHis1, and the axial water molecule is displaced
253 (Fig. 6b and 6d). The identity of the glycosyl unit at subsite -3 is ambiguous though best
254 modelled as mannose. The density of the glycosyl unit at subsite -4 is weak and occupies
255 a very similar position as the corresponding unit in the *LsAA9A*:Cell₆ complex, as does the
256 glycosyl unit at subsite -3 , due to similar crystal constraints.

257 *Complexes with xylo-oligosaccharide*

258 Whereas in crystals soaked with Xyl₃ and Xyl₄ (Supplementary Tables 2–5) the
259 oligosaccharides did not fully span the active site, *LsAA9A*:Xyl₅ crystals revealed very well-
260 defined density from subsites -3 to $+2$ (Fig. 7a). The oligosaccharide position at subsites
261 -3 to -1 are similar to *LsAA9A*:Cell₅, but with a translation of about half a pyranose unit in
262 the non-reducing end direction. In contrast, the plane of the xyloside unit at subsite $+1$ is
263 rotated approximately 90° compared to the corresponding glucosidic unit, while the
264 xyloside residue binding $+2$ is rotated approximately 180° (Fig. 7d, Supplementary Table
265 2). As a result xylose at subsite $+1$ does not stack with MeHis1, and in fact appears to
266 have no interactions with the enzyme, while the same residues that bind the subsite $+2$
267 glucosyl residue in the *LsAA9A*:Cell₅ structure, Asn28, His66 and Asn67, interact here with
268 O1, O5 and O1 of the $+2$ xyloside residue, respectively (Fig. 7c Supplementary Table 3). A
269 structure of *LsAA9A*:Xyl₅ determined from a low X-ray dose data collection showed the
270 substrate bound similarly, and revealed a mix of water/Cl⁻ in the axial position and a fully
271 occupied equatorial water on the active site copper (Fig. 7b). Thus, in contrast to binding

272 of cello- or glucomannan oligosaccharides, the axial water was not displaced by binding of
273 Xyl₅.

274 **EPR data suggest alternative *LsAA9A* substrate binding modes**

275 We studied substrate binding on both *LsAA9A* and *CvAA9A* using electron paramagnetic
276 resonance (EPR) spectroscopy (Table 2) to investigate the electronic state of the active
277 site copper upon binding. As has been shown by Frandsen et al.³³ and Courtade et al.²¹, the
278 binding affinity of oligosaccharide substrates is significantly affected by the presence of the
279 exogenous ligand on the copper ion. Accordingly, EPR experiments were carried out in
280 both the absence and presence of 200 mM chloride (1.0 M chloride for Xyl₆ studies).
281 Furthermore, experiments were carried out at high substrate concentration to maximize
282 substrate binding. For *LsAA9A* a wide range of substrates was tested. In all cases, the
283 parallel region of the spectra could be modelled with reliable g_z and $|A_z|$ values, giving
284 some insight into the electronic nature of the copper ion. Perpendicular values were less
285 reliable due to the second-order nature of the spectra in this region, and are therefore not
286 used in the analysis, although the appearance of superhyperfine coupling to ligands in this
287 region was apparent in some cases (Table 2, Supplementary Fig. 12) and used as an
288 indication of increased metal-ligand covalency in the singly-occupied molecular orbital
289 (SOMO), as previously discussed by Frandsen et al.³³. In all cases apart from xylan, the
290 addition of substrate gave perturbation of the Cu spin Hamiltonian parameters similar to
291 that already reported by Frandsen et al.³³ In particular, shifts in g_z values to ca 2.23 (along
292 with the appearance of strong superhyperfine coupling) were seen upon addition of Avicel,
293 glucomannan and xyloglucan, indicative of chloride coordination to the copper ion in the
294 equatorial position of the copper coordination sphere. These shifts are analogous to those
295 of *LsAA9A* interacting with Cell₆ and PASC³³. In contrast, addition of Xyl₆ did not give
296 significant shifts in g_z but did give perturbations in the $|A_z|$ value, with the appearance of
297 superhyperfine coupling indicative of a second species different from that formed with
298 Cell₆. The EPR spectra of *LsAA9A* binding to Xyl₆ and xylan are indicative of substrate
299 binding to the enzyme (although binding of Xyl₆ could be achieved only at high chloride
300 concentrations), but without the chloride occupying the equatorial coordination position on
301 the copper ion, revealing that these substrates drive an electronic state at the copper ion
302 that is different to that of the other substrates. EPR perturbation was seen upon addition of

303 Cell₆ to CvAA9A but not with Xyl₆, consistent with the observed activity on Cell₆ and not
304 Xyl₆ (Fig.8 and Supplementary Fig.13).

305

306 **Discussion**

307 Our understanding of the molecular basis for substrate binding and cleavage has been
308 aided by the recent report of a crystal structure of *LsAA9A* in complex with Cell₃ and Cell₆,
309 as well as biochemical and EPR data for *LsAA9A* on cellulosic substrates³³. Here, we have
310 extended this biochemical, EPR and structural analysis by using a range of substrates as
311 well as an additional related enzyme, *CvAA9A*, to provide a better insight into substrate
312 specificity.

313 Extensive probing of *LsAA9A* and *CvAA9A* substrate specificity showed that both cleave a
314 range of cellulosic and non-cellulosic substrates, some of which have been shown for
315 other AA9s^{19,20,22,23,27,29,35,39-41}. We made a number of novel observations. Notably,
316 *LsAA9A* activity on xylan and xylo-oligosaccharides is the first report of LPMO cleavage of
317 isolated xylan; this may have important implications for the use of LPMOs in
318 biotechnological contexts. LPMO activity on xylan has been observed before for
319 *MtLPMO9A*²³, but only on xylan associated with cellulose. We also observe that both
320 *LsAA9A* and *CvAA9A* are able to cleave glycosidic bonds adjacent to mannosyl residues
321 (Supplementary Fig. 6), which occur interspersed randomly with glucosyl residues in
322 glucomannan, a biochemical observation supported by the *LsAA9A*:glucomannan
323 oligosaccharide structure, which unambiguously shows a mannosyl residue at subsite +1.
324 We also noticed substrate-specific oxidation profiles, namely that *LsAA9A* and *CvAA9A*
325 cleaved small oligosaccharides using a C4-oxidising mechanism whereas they cleaved
326 polysaccharides with both C1- and C4-oxidising mechanisms in varying proportions.
327 Assuming a copper-based oxidative species, the similar distances between both C1 and
328 C4 axial protons and the active oxygen species, as noted in Frandsen et al.³³, may allow
329 slight differences in substrate binding to switch the C-H bond that is closest to attack.
330 Substrate binding differences may also subtly alter the electronics at the copper site, which
331 potentially could also favour a specific oxidation site. Oxidation regioselectivity is therefore

332 less likely to be a strong functional constraint. This is in agreement with the presence of
333 C1 and C4 regiospecificity in several clades in the N-terminal sequence similarity tree (Fig.
334 1). On the other hand, the tree enabled us successfully to predict that *LsAA9A* and
335 *CvAA9A* might have similarities in having activity on a range of soluble substrates.

336 Our investigation highlighted many examples of the way in which substrate specificity and
337 the site of attack on a polysaccharide is dictated by binding cleft interactions with the
338 substrate. For example, *LsAA9A*'s preference to cleave Cell₄ into Cell₂ (as shown for
339 *NcLPMO9C*¹⁸), compared to the product profile of *CvAA9A* of Cell₃, Cell₂ and Glc
340 (Supplementary Fig. 5), could be attributed to binding cleft interactions at the +2 subsite.
341 This is because though *CvAA9A* shares the same fold, active site co-ordination and overall
342 structure with *LsAA9A*, it lacks all three of the subsite +2 substrate-binding residues in
343 *LsAA9A* (Asn28, His66 and Asn67) (Fig. 5; Supplementary Fig. 1). This suggests that,
344 while *LsAA9A* binds Cell₄ from subsite -2 to +2, *CvAA9A* binds between subsites -3 and
345 +1.

346 The structural data provide a molecular rationale for how *LsAA9A* is able to catalyse the
347 unexpected cleavage of mannose-containing bonds. The *LsAA9A*:glucomannan
348 oligosaccharide crystal structure shows the presence of a mannose (the C2 epimer of
349 Glc), and essentially no Glc, at subsite +1. Talose (C4 epimer of mannose) and galactose
350 (C4 epimer of Glc) arose from the reduction of C4-oxidised cleavage products
351 (Supplementary Fig. 6), also suggesting both mannosyl and glucosyl occupation of subsite
352 +1. We have previously described that the glucosyl unit at the +1 subsite in *LsAA9A* Cell₃
353 and Cell₆ complexes^{33,38} interacts with MeHis1 through its β -face, and while glucose can
354 make carbohydrate-aromatic stacking interactions⁴² through both faces of the pyranose
355 ring, β -mannose is believed to have absolute preference for interactions through its α -face
356 due to its axial C2-hydroxyl. Nonetheless, determination of the crystal structure of
357 glucomannan fragments with *LsAA9A* confirmed that this type of interaction takes place,
358 and the mannosyl residue at the +1 subsites interacts with MeHis through its β -face with
359 an O5-imidazole ring centre distance of 3.6 Å (Fig 6d) (compared to 3.4-3.5 Å for the cello-
360 oligosaccharide complexes). No similar interactions could be found through a search in the
361 PDB. We did not observe a mannosyl residue at the -1 subsite in the structure, but it

362 would cause no steric clash and so could be readily accommodated (though it would
363 cause the loss of a hydrogen bond interaction with Ser77).

364 Although we were unable to obtain a structure with xyloglucan oligosaccharides bound,
365 our observation that both *LsAA9A* and *CvAA9A* cleaved xyloglucan DP14–18 oligomers
366 with the sole unsubstituted backbone glucosyl residues at subsite +1 (XXX/GXXXGol; as
367 found for *NcLPMO9C*¹⁹) is consistent with the binding of xyloglucan's cellulose backbone
368 being similar to the binding of cello-oligosaccharides. This would suggest that the *LsAA9A*
369 could tolerate glucosyl residues with C6 xylosyl substitutions at subsites –1 or +2, but not
370 at +1 where the C6 hydroxymethyl group occludes the copper axial binding site, and
371 displaces the axial water.

372 *LsAA9A* under the selected conditions degraded Xyl₆ with about 1/100 the efficiency as
373 Cell₆, while *CvAA9A* left Xyl₆ essentially untouched at all conditions tested (Supplementary
374 Fig. 9). The differences in key amino acids involved in defining the *LsAA9A* and *CvAA9A*
375 subsites, particularly the +2 subsite (vide supra) (Supplementary Fig. 1; Fig. 5), are likely
376 an important factor in *LsAA9A*'s superior xylan-degrading activity.

377 Our observation in *LsAA9A* complexes that MLG oligosaccharides were unable to bind
378 with β -(1→3)-glucan bonds near the active site are consistent with our observation that
379 both *LsAA9A* and *CvAA9A* favour the cleavage of cellulose regions in MLG.

380 Not all aspects of substrate specificity could be explained through binding cleft
381 interactions. Rather, aspects of the specificity differences appear to be mechanistic in
382 origin and relate to the reactivity of different substrates. The high activity, spectroscopy
383 data and structures of *LsAA9A* and *CvAA9A* with β -(1→4)-glucan substrates leads us to
384 suggest the effective oxidative mechanism deployed in these situations may be regarded
385 as a 'canonical pathway'. It is clear, however, that LPMOs may also have other 'non-
386 canonical pathway' mechanisms, as exemplified by the differences between binding,
387 spectroscopy and structures of *LsAA9A* with Xyl₆. The crystallographic and EPR data show
388 that a chloride ion – an oxygen species mimic – is not recruited into the copper's equatorial
389 binding site upon xylooligosaccharide substrate binding, as happens in the canonical
390 mechanism described by Frandsen et al³³. The aldopentose nature of xylose categorically
391 excludes the synergistic binding of saccharide ligand and molecular oxygen which is

392 brought about by a bridging “pocket” water molecule between the C6-hydroxymethyl group
393 of Glc and the amino terminus of the enzyme. This suggests a different oxidative
394 mechanism may well be in operation for the cleavage of xylose-based substrates by
395 *LsAA9A*. Indeed, as has already been proposed by Kjaergaard et al⁴³, activation of O₂ by
396 an AA9 from *Thermoascus aurantiacus* probably gives formation of a copper-bound
397 superoxide or hydrosuperoxide (HO₂) through associative displacement of a superoxide
398 anion by a water molecule through the axial coordination site on the copper ion. In
399 particular, a superoxide ion bound to the copper in the axial position would be in position to
400 cleave a saccharidic chain by direct attack. Such a mechanism is expected when the axial
401 water molecule on the copper ion is *not* displaced by the binding of substrate, as is the
402 case with the binding of Xyl₅ to *LsAA9A*. From the low dose *LsAA9A*:Xyl₅ structure
403 described herein, the axial ligand is clearly present on the copper ion, though it is best
404 modelled as a mixture of chloride and water, and the Tyr-O distance (2.86 Å) is not
405 shortened compared to the un-complexed low dose structure (2.72Å - PDB 5ACG). This is
406 in contrast to the low dose *LsAA9A*:Cell₃ structure where the Tyr-O distance is 2.47 Å
407 (PDB 5ACF). Furthermore, the equatorial position in the low dose *LsAA9A*:Xyl₅ is occupied
408 by a water molecule, not a chloride ion, as corroborated by the EPR spectroscopy. Thus, a
409 mechanism by which a copper-bound superoxide is generated next to the substrate is
410 possible within the *LsAA9A*-Xyl₅ complex. Such a mechanism may be expected to be rate-
411 independent on the redox potential of the reducing agent, since the rate-limiting step is
412 likely to be hydrogen atom abstraction by the superoxide from the substrate rather than
413 reductive cleavage of the O-O bond. Therefore, the fact that the rate of cleavage of xylan
414 and Xyl₆ by *LsAA9A* is less dependent on reducing agent while the cleavage of the other
415 substrates is strongly dependent (Figure 4) illustrates that a different oxidative mechanism
416 is in operation. Thus the extent of activity on certain substrates is a function of the
417 oxidative species which can be formed at the copper ion which is—in turn—dependent on
418 the substrate. This means that for some substrates the use of reducing agents with
419 different potentials can profoundly affect apparent substrate specificity. But, more
420 importantly, LPMOs appear to have more than one oxidative mechanism available for
421 substrate cleavage, governed to some extent by the nature of the substrate-LPMO
422 interaction. Indeed, the existence of multiple oxidative mechanisms for a single LPMO is
423 an intriguing contribution to the on-going debate about LPMO mode of action. Results

424 obtained in this study broaden the known substrate specificity of AA9 LPMOs to include
425 isolated xylan and xylo-oligosaccharides, and mannosyl-containing bonds within
426 glucomannan. We further show that oxidation type (C1/C4) is influenced by substrate type,
427 and in this work differed between oligo- and polysaccharides. This investigation into the
428 molecular causes of AA9 LPMO substrate specificity demonstrated the existence of
429 multiple influences. As with carbohydrate-acting hydrolases, for example, LPMO substrate
430 specificity is dictated by binding cleft protein:carbohydrate interactions. But in addition, the
431 fact that activity on some substrates is differentially responsive to reducing agent potential
432 suggests that these carbohydrates do not properly activate the active site copper, and are
433 cleaved through an alternative oxidative pathway. Combinations of canonical and non-
434 canonical mechanisms greatly extend the range of potential substrates for LPMOs and
435 offer new insight into their biochemical mode of action.

436

437 **Materials and methods**

438 *Phylogenetic tree*

439 AA9 is a family with more than 6000 sequences listed in NCBI nr and JGI databases in
440 2016. Because of high variability in the N-terminal portion of LPMO amino acid sequences,
441 no significant global alignment of LPMOs can be obtained – thereby limiting global
442 downstream phylogenetic analyses. We chose therefore to extract the highly variable N-
443 terminal half of these sequences (which includes two histidine residues involved in the
444 coordination of the copper atom) for phylogenetic analysis as well as to limit the analysis to
445 sequences that are closely related to each other and to those that have been
446 biochemically characterized in the literature. We reduced the set of AA9 sequences to
447 those that gave BLAST bit-scores greater than or equal to a value of 200, using *LsAA9A*
448 and *TaAA9A* as queries. A Jaccard distance matrix was compiled from BLAST bit scores
449 and represented as a tree, built according to the principle of neighbor-joining method⁴⁴
450 displaying the resulting 444 sequences (Fig. 1).

451 *Protein production*

452 Cloning, expression, and purification of *LsAA9A* was done as described previously³³. The
453 gene encoding *CvAA9A* was amplified from genomic DNA of *Collariella virescens*
454 (formerly known as *Chaetomium virescens*) and expressed in *Aspergillus oryzae* MT3568.
455 The secreted LPMO was purified using a Butyl Toyopearl resin followed by purification on
456 a Q-Sepharose FF resin followed by ultrafiltration with 10 kDa cutoff filter.

457 *Enzyme assays*

458 Apo-*LsAA9A* and apo-*CvAA9A* were pre-incubated for 0.5–1 h at 5 °C in 0.9 stoichiometric
459 Cu(II)(NO₃)₂ immediately before enzyme reactions. AA9 enzyme reactions on
460 oligosaccharides were in 10 µL containing 5 nmol oligosaccharide, 100 mM ammonium
461 formate pH 6, ±4 mM ascorbate, pyrogallol or cysteine, ±5 pmol *LsAA9A* or *TaAA9A* and
462 were incubated at 20 °C for 4 h. Xyloglucan endoglucanase (XEG) reactions were in 10 µL

463 containing 5 nmol oligosaccharide, 100 mM ammonium formate pH 6, ± 10 μmol GH5 XEG
464 and were incubated at 20 °C for 4 h. Oligosaccharides were purchased from Megazyme
465 (see also following section). In general, enzyme reactions on polysaccharides were in 100
466 μL containing 0.5% (w/v) polysaccharide, 100 mM ammonium formate pH 6, ± 4 mM
467 ascorbate, pyrogallol or cysteine, ± 63 pmol LPMO, and were incubated at 20 °C for 16 h.
468 Avicel cellulose was purchased from Sigma-Aldrich, UK; barley beta-glucan medium
469 viscosity (mixed-linkage glucan), konjac glucomannan, tamarind xyloglucan, birchwood
470 xylan, corn starch and laminarin were purchased from Megazyme, Ireland; squid-pen β -
471 chitin was a kind gift from Dominique Gillet of Mahtani Chitosan. Phosphoric acid-swollen
472 cellulose (PASC) was prepared as described previously³³. Mixed-linkage glucan,
473 glucomannan, xyloglucan, xylan, starch and laminarin were boiled for 5 mins to make
474 solubilized 1% (w/v) stock solutions before reactions. To aid solubilisation where
475 necessary, water was added to a methanol: polysaccharide slurry before boiling, which
476 improved dispersion throughout the water. Reactions were routinely stopped by addition of
477 three reaction volumes of 96% (v/v) ethanol before precipitation of the undigested
478 substrates, and separation of the reaction products for further analysis. Polysaccharide
479 Analysis by Carbohydrate Electrophoresis (PACE) using high concentration acrylamide
480 gels (for resolution of small oligosaccharides) and lower concentration gels (for resolution
481 of larger oligosaccharides) was carried out as described by Frandsen et al.³³ and Goubet
482 et al.⁴⁵ respectively. MALDI-ToF MS was performed as described previously⁴⁶. 2-
483 Aminobenzamide (2-AB) labelling was performed as described previously³³. All
484 experiments were carried out at least three times.

485 Sodium borohydride reducing agent experiments were performed as described by
486 Frandsen et al.³³. HPAEC was performed on a CarboPac PA1 column (Dionex) with
487 injections of 20 μL and elution at 0.4 mL min⁻¹. The elution profile was: 0–3 min, 10 mM
488 NaOH (isocratic); 3–6 min, 10→1 mM NaOH (linear gradient); 6–19 min, 1 mM NaOH
489 (isocratic); 19–37 min, 45 mM NaOH, 225 mM sodium acetate (isocratic). A pulsed
490 amperometric detector (PAD) with a gold electrode was used. PAD response was
491 calibrated using markers (500 pmol).

492 *X-ray crystallography and PDB database searches*

493 All crystallization trials were set up in MRC 2-well plates at room temperature using an
494 Oryx-8 robot (Douglas Instrument). Crystals were obtained by sitting-drop vapor diffusion
495 technique in drops of 0.3-0.5 μL with a reservoir volume of 100 μL . Pre-incubation with 1-2
496 mM Cu(II) acetate for 30-60 min was carried out for all crystallization trials. Crystallization
497 and post-crystallization experimental details are shown in Supplementary Table 4. Crystals
498 were cryocooled in liquid nitrogen and all datasets were collected at cryogenic
499 temperatures (100 K) at either the MX beamlines I911-2/I911-3 at MAX-lab in Lund,
500 Sweden, or at the MX beamlines ID23-1, ID23-2 or ID30-B at ESRF, Grenoble, France
501 (Supplementary Table 5). *LsAA9A* crystallization was performed as described in Frandsen
502 et al.³³. Oligosaccharide substrates used for soaking were purchased from Megazyme
503 (MLG (G4G4G3G and G4G3G4G), xylotriose (*Xyl*₃), xyloetraose (*Xyl*₄), xylopentaose
504 (*Xyl*₅), xyloglucan heptasaccharide (XXXG), cellotriose (*Cell*₃) or provided by Novozymes
505 A/S (cellopentaose (*Cell*₅)). Data were initially collected on crystals soaked with G4G4G3G
506 (*LsAA9A*:G4G4G3G; PDB 5NLR), *Xyl*₃ (*LsAA9A*:*Xyl*₃; PDB 5NLQ), *Xyl*₄ (*LsAA9A*:*Xyl*₄;
507 PDB 5NLP) and *Cell*₅ (*LsAA9A*:*Cell*₅; 5NLS). On a crystal soaked with *Xyl*₅ a dataset with
508 reduced X-ray dose ((*LsAA9A*:*Xyl*₅Cu(II); PDB 5NLN; 40 frames of 5.7% transmission,
509 0.05s exposure/frame, 1° oscillation with a beamsize of 10x10 μm) was collected using
510 helical collection to minimize photoreduction of the active site copper. Subsequently, on
511 similar crystals another full dose dataset was collected to high resolution (*LsAA9A*:*Xyl*₅;
512 PDB 5NLO). Ladders of glucomannan (GM), from konjac, and of xyloglucan (XG), from
513 tamarind, were prepared by partial acid hydrolysis (20-200 mM TFA for 20 min at 120°C)
514 of polysaccharide substrates purchased from Megazyme. Hydrolyzed products were
515 isolated using ethanol precipitation to remove the remaining polysaccharides. The
516 oligosaccharides were dried thoroughly using a SpeedVac. Data were collected on crystals
517 soaked in GM (*LsAA9A*:GM; PDB 5NKW) or XG stock solutions (in 3.8 M NaCl, 0.1 M
518 citric acid pH 5.5). Crystals were also soaked in the presence of 0.3 M XXXG, and up to
519 1.2 M of XG oligosaccharide purchased from Megazyme (consisting primarily of
520 XXXGXXXG, see Courtade et al.²¹). No complex structures were obtained from any of the
521 crystals soaked with XG substrates, either because no binding was observed or only
522 cellooligosaccharides were bound (presumably because acid hydrolysis caused
523 debranching).

524 *CvAA9A* was deglycosylated in 20 mM MES, pH 6.0, 125 mM NaCl by incubation with
525 approximately 0.03 units mg⁻¹ *CvAA9A* of endoglycosidase H from (Roche Diagnostics,
526 11643053001), and then buffer exchanged to 20 mM Na-acetate pH 5.5. Intergrown
527 crystals were initially obtained in an index screen in conditions of 1.5–2.0 M (NH₄)₂SO₄
528 (and in some cases 0.1 M NaCl) in pH 6.5–8.5 (0.1 M of either Bis-Tris, HEPES or Tris).
529 The crystals diffracted to 2.0–3.5 Å resolution but were multiple. Crystal conditions were
530 optimized in a range of 1.2 M – 2.6 M (NH₄)₂SO₄ (+/- 0.1 M NaCl) in pH 6.5–8.5, which
531 produced crystal plates suitable for mounting. A dataset collected at I911-3 on a crystal
532 grown in 0.1 M Bis-Tris pH 6.5, 2.0 M (NH₄)₂SO₄ could be processed in *P2*₁ to 2.5 Å (PDB
533 5NLT). A preliminary *CvAA9A* structure with four molecules in the asymmetric unit was
534 solved by Molecular Replacement using MOLREP with modified coordinates of the high
535 resolution structure of *LsAA9A* (PDB 5ACH) which is 41% identical, as a model and
536 refined isotropically to an R_{free} of 32%. From another dataset (collected on a crystal grown
537 in presence of 0.1 M NaCl; Supplementary Table 4) a structure solved (using the
538 preliminary one) with six molecules in the asymmetric unit could be fully modelled and
539 refined resulting in the complete *CvAA9A* structure (Supplementary Table 5). The 6
540 molecules in the asymmetric unit are very similar (average RMSDs of 0.08Å). The density
541 of MeHis1 is less clear in chains C and F, and in particular methylation is not as obvious in
542 all chains. Soaks (with 1.2 M Cell₃) of *CvAA9A* were also prepared. Data were collected to
543 2.1 Å and the electron density showed a Cell₃ molecule, which however was not bound at
544 the active site (not shown). Soaks with Cell₆ damaged the crystals.

545 Each dataset was processed using XDS (the resolution cutoff was chosen on the basis of
546 a CC_{1/2} around 50%) and subsequently scaled using XSCALE. Refmac5 was used for
547 restrained refinement of the structures in which *LsAA9A*:Xyl₅ was refined anisotropically,
548 while *LsAA9A*:Xyl₃ was refined anisotropically for protein atoms and isotropically for all
549 other atoms. All other structures were refined isotropically for all atoms. For
550 *LsAA9A*:G4G4G3G the structure was best modelled by the G4G4G portion of the
551 substrate bound mainly in subsite -1 to +2 (80% occupancy) and with a minor
552 conformation occupying subsite -2 to +1 (20% occupancy). Near subsite -2 a number of
553 water molecules were modelled with 80% occupancy. Ligands and structures were
554 modelled in COOT and validated using MolProbity (within COOT) and Procheck (CCP4
555 suite) which reported Ramachandran plots with 99% of residues in allowed regions for all

556 structures. Scaled data statistics and refinement statistics are summarized in
557 Supplementary Table 5.

558 To identify potential stacking interactions of the β -face of β -mannose with His, the PDB
559 database was searched with Glyvicinity⁴⁷. First all protein/ β -mannose interactions within a
560 distance cut-off of 4.0 Å for structures determined at a resolution better than 3.0 Å were
561 identified. Among these, only two structures were found where the interactions involved
562 His residues and the pyranose O5. The interactions between the imidazole and the
563 pyranose rings were side by side or almost perpendicular, and thus not comparable with
564 the +1 subsite interactions of the *LsAA9A* complexes.

565

566 *Electron Paramagnetic Resonance (EPR) Spectroscopy*

567

568 Continuous wave (cw) X-band frozen solution EPR spectra of 0.2 to 0.3 mM solution of
569 *LsAA9A* or *CvAA9A* (in 10% v/v glycerol) at pH 6.0 (50 mM sodium phosphate buffer with
570 or without addition of 200 mM NaCl or 20 mM MES buffer, 200 mM NaCl) and 165 K were
571 acquired on a Bruker EMX spectrometer operating at ~9.30 GHz, with modulation
572 amplitude of 4 G, modulation frequency 100 kHz and microwave power of 10.02 mW (3
573 scans). Avicel cellulose, konjac glucomannan, tamarind xyloglucan and birchwood xylan
574 were added to the EPR tube containing the protein as solids. Alternatively, glucomannan
575 and xylan were heated until dissolution (*ca.* 2 min) to make solubilized 1% (w/v) stock
576 solutions in water, which were then used for addition of excess polysaccharide to *LsAA9A*.
577 Cellohexaose and xylohexaose were added to the protein solution either from stock
578 solutions in water or as a solid up to 60 or 150-fold excess, respectively. For the
579 experiments in the presence of xylohexaose, additional NaCl was added to the protein
580 alone or the protein:Xyl₆ mixture from a 5 M stock solution. Due to the high amount of
581 protein required by the technique, the data presented are from single EPR experiments,
582 although the spectra with Cell₆, Xyl₆ and avicel were performed in at least duplicate.

583 Spectral simulations were carried out using EasySpin 5.0.3⁴⁸ integrated into MATLAB
584 R2016a⁴⁹ software on a desktop PC. Simulation parameters are given in Table 2. g_z and
585 $|A_z|$ values were determined accurately from the absorptions at low field. It was assumed
586 that g and A tensors were axially coincident.

587

588 *Data availability*

589

590 Protein Data Bank: Atomic coordinates and structure factors for the reported crystal
591 structures were deposited under accession codes 5NLT (*CvAA9A*), 5NLS (*LsAA9A-Cell₅*),
592 5NLR (*LsAA9A-G4G4G3G*), 5NKW (*LsAA9A-GM*), 5NLQ (*LsAA9A-Xyl₃*), 5NLP (*LsAA9A-*
593 *Xyl₄*), 5NLO (*LsAA9A-Xyl₅*) and 5NLN (*LsAA9A-Xyl₅-Cu_{II}*), GenBank: Sequence data for
594 *CvAA9A* were deposited under accession code KY884985. Raw EPR data are available
595 on request through the Research Data York (DOI: 10.15124/5810c962-148c-4328-ab92-
596 895e2dae4d3c).

597

598 **References**

- 599 1 Carroll, A. & Somerville, C. Cellulosic Biofuels. *Annu. Rev. Plant Biol.* **60**, 165-182, (2009).
600 2 Perlack, R. D. & Stokes, B. J., Leads. *U.S. Billion-Ton Update: Biomass Supply for a Bioenergy and*
601 *Bioproducts Industry*. Technical Report ORNL/TM-2011/224, 227. (U.S. Department of Energy, Oak
602 Ridge National Laboratory, Oak Ridge, TN, 2011).
603 3 Marriott, P. E., Gomez, L. D. & McQueen-Mason, S. J. Unlocking the potential of lignocellulosic
604 biomass through plant science. *New Phytol.* **209**, 1366-1381, (2016).
605 4 Simmons, T. J. *et al.* Folding of xylan onto cellulose fibrils in plant cell walls revealed by solid-state
606 NMR. *Nat. Commun.* **7**, (2016).
607 5 Correa, T. L. R., dos Santos, L. V. & Pereira, G. A. G. AA9 and AA10: from enigmatic to essential
608 enzymes. *Appl. Microbiol. Biot.* **100**, 9-16, (2016).
609 6 Muller, G., Varnai, A., Johansen, K. S., Eijsink, V. G. H. & Horn, S. J. Harnessing the potential of
610 LPMO-containing cellulase cocktails poses new demands on processing conditions. *Biotechnol.*
611 *Biofuels* **8**, (2015).
612 7 Hemsworth, G. R., Henrissat, B., Davies, G. J. & Walton, P. H. Discovery and characterization of a
613 new family of lytic polysaccharide monooxygenases. *Nat. Chem. Biol.* **10**, 122-126, (2014).
614 8 Cantarel, B. L. *et al.* The Carbohydrate-Active EnZymes database (CAZy): an expert resource for
615 Glycogenomics. *Nucleic Acids Res.* **37**, D233-D238, (2009).
616 9 Lombard, V., Ramulu, H. G., Drula, E., Coutinho, P. M. & Henrissat, B. The carbohydrate-active
617 enzymes database (CAZy) in 2013. *Nucleic Acids Res.* **42**, D490-D495, (2014).
618 10 Vu, V. V., Beeson, W. T., Span, E. A., Farquhar, E. R. & Marletta, M. A. A family of starch-active
619 polysaccharide monooxygenases. *P. Natl. Acad. Sci. USA* **111**, 13822-13827, (2014).
620 11 Lo Leggio, L. *et al.* Structure and boosting activity of a starch-degrading lytic polysaccharide
621 monooxygenase. *Nat. Commun.* **6**, (2015).
622 12 Quinlan, R. J. *et al.* Insights into the oxidative degradation of cellulose by a copper metalloenzyme
623 that exploits biomass components. *P. Natl. Acad. Sci. USA* **108**, 15079-15084, (2011).
624 13 Hemsworth, G. R., Johnston, E. M., Davies, G. J. & Walton, P. H. Lytic Polysaccharide
625 Monooxygenases in Biomass Conversion. *Trends Biotechnol.* **33**, 747-761, (2015).
626 14 Vaaje-Kolstad, G., Horn, S. J., van Aalten, D. M. F., Synstad, B. & Eijsink, V. G. H. The non-catalytic
627 chitin-binding protein CBP21 from *Serratia marcescens* is essential for chitin degradation. *J. Biol.*
628 *Chem.* **280**, 28492-28497, (2005).

629 15 Merino, S. T. & Cherry, J. Progress and challenges in enzyme development for Biomass utilization.
630 *Adv. Biochem. Eng. Biot.* **108**, 95-120, (2007).

631 16 Harris, P. V. *et al.* Stimulation of Lignocellulosic Biomass Hydrolysis by Proteins of Glycoside
632 Hydrolase Family 61: Structure and Function of a Large, Enigmatic Family. *Biochemistry-Us* **49**,
633 3305-3316, (2010).

634 17 Vaaje-Kolstad, G. *et al.* An Oxidative Enzyme Boosting the Enzymatic Conversion of Recalcitrant
635 Polysaccharides. *Science* **330**, 219-222, (2010).

636 18 Isaksen, T. *et al.* A C4-oxidizing Lytic Polysaccharide Monooxygenase Cleaving Both Cellulose and
637 Cello-oligosaccharides. *J. Biol. Chem.* **289**, 2632-2642, (2014).

638 19 Agger, J. W. *et al.* Discovery of LPMO activity on hemicelluloses shows the importance of oxidative
639 processes in plant cell wall degradation. *P. Natl. Acad. Sci. USA* **111**, 6287-6292, (2014).

640 20 Bennati-Granier, C. *et al.* Substrate specificity and regioselectivity of fungal AA9 lytic polysaccharide
641 monooxygenases secreted by *Podospira anserina*. *Biotechnol. Biofuels* **8**, (2015).

642 21 Courtade, G. *et al.* Backbone and side-chain H-1, C-13, and (15) N chemical shift assignments for the
643 apo-form of the lytic polysaccharide monooxygenase NcLPMO9C. *Biomol. NMR Assign.* **10**, 277-280,
644 (2016).

645 22 Jagadeeswaran, G., Gainey, L., Prade, R. & Mort, A. J. A family of AA9 lytic polysaccharide
646 monooxygenases in *Aspergillus nidulans* is differentially regulated by multiple substrates and at
647 least one is active on cellulose and xyloglucan. *Appl. Microbiol. Biot.* **100**, 4535-4547, (2016).

648 23 Frommhagen, M. *et al.* Discovery of the combined oxidative cleavage of plant xylan and cellulose by
649 a new fungal polysaccharide monooxygenase. *Biotechnol. Biofuels* **8**, (2015).

650 24 Levasseur, A., Drula, E., Lombard, V., Coutinho, P. M. & Henrissat, B. Expansion of the enzymatic
651 repertoire of the CAZy database to integrate auxiliary redox enzymes. *Biotechnol. Biofuels* **6**,
652 (2013).

653 25 Yakovlev, I. *et al.* Substrate-specific transcription of the enigmatic GH61 family of the pathogenic
654 white-rot fungus *Heterobasidion irregulare* during growth on lignocellulose. *Appl. Microbiol. Biot.*
655 **95**, 979-990, (2012).

656 26 Poidevin, L. *et al.* Comparative analyses of *Podospira anserina* secretomes reveal a large array of
657 lignocellulose-active enzymes. *Appl. Microbiol. Biot.* **98**, 7457-7469, (2014).

658 27 Frommhagen, M. *et al.* Lytic polysaccharide monooxygenases from *Myceliophthora thermophila* C1
659 differ in substrate preference and reducing agent specificity. *Biotechnol. Biofuels* **9**, (2016).

660 28 Kracher, D. *et al.* Extracellular electron transfer systems fuel cellulose oxidative degradation.
661 *Science* **352**, 1098-1101, (2016).

662 29 Borisova, A. S. *et al.* Structural and Functional Characterization of a Lytic Polysaccharide
663 Monooxygenase with Broad Substrate Specificity. *J. Biol. Chem.* **290**, 22955-22969, (2015).

664 30 Frandsen, K. E. H. & Lo Leggio, L. Lytic polysaccharide monooxygenases: a crystallographer's view
665 on a new class of biomass-degrading enzymes. *Lucrij* **3**, 448-467, (2016).

666 31 Vaaje-Kolstad, G., Forsberg, Z., Loose, J. S., Bissaro, B. & Eijsink, V. G. Structural diversity of lytic
667 polysaccharide monooxygenases. *Curr Opin Struct Biol* **44**, 67-76, (2017).

668 32 Davies, G. J., Wilson, K. S. & Henrissat, B. Nomenclature for sugar-binding subsites in glycosyl
669 hydrolases. *Biochem J* **321 (Pt 2)**, 557-559, (1997).

670 33 Frandsen, K. E. H. *et al.* The molecular basis of polysaccharide cleavage by lytic polysaccharide
671 monooxygenases. *Nat. Chem. Biol.* **12**, 298+, (2016).

672 34 Walton, P. H. & Davies, G. J. On the catalytic mechanisms of lytic polysaccharide monooxygenases.
673 *Curr. Opin. Chem. Biol.* **31**, 195-207, (2016).

674 35 Cannella, D. *et al.* Light-driven oxidation of polysaccharides by photosynthetic pigments and a
675 metalloenzyme. *Nat. Commun.* **7**, (2016).

676 36 Lenfant, N. *et al.* A bioinformatics analysis of 3400 lytic polysaccharide oxidases from family AA9.
677 *Carbohydr Res*, (2017).

- 678 37 Loose, J. S. M. *et al.* Activation of bacterial lytic polysaccharide monoxygenases with cellobiose
679 dehydrogenase. *Protein Sci.* **25**, 2175-2186, (2016).
- 680 38 Frandsen, K. E. H., Poulsen, J. C. N., Tovborg, M., Johansen, K. S. & Lo Leggio, L. Learning from
681 oligosaccharide soaks of crystals of an AA13 lytic polysaccharide monoxygenase: crystal packing,
682 ligand binding and active-site disorder. *Acta Crystallogr. D.* **73**, 64-76, (2017).
- 683 39 Kojima, Y. *et al.* A Lytic Polysaccharide Monoxygenase with Broad Xyloglucan Specificity from the
684 Brown-Rot Fungus *Gloeophyllum trabeum* and Its Action on Cellulose-Xyloglucan Complexes. *Appl.*
685 *Environ. Microb.* **82**, 6557-6572, (2016).
- 686 40 Nekiunaite, L., Arntzen, M. O., Svensson, B., Vaaje-Kolstad, G. & Abou Hachem, M. Lytic
687 polysaccharide monoxygenases and other oxidative enzymes are abundantly secreted by
688 *Aspergillus nidulans* grown on different starches. *Biotechnol. Biofuels* **9**, (2016).
- 689 41 Fanuel, M. *et al.* The *Podospora anserina* lytic polysaccharide monoxygenase PaLPMO9H catalyzes
690 oxidative cleavage of diverse plant cell wall matrix glycans. *Biotechnol Biofuels* **10**, 63, (2017).
- 691 42 Asensio, J. L., Arda, A., Canada, F. J. & Jimenez-Barbero, J. Carbohydrate-Aromatic Interactions.
692 *Accounts Chem. Res.* **46**, 946-954, (2013).
- 693 43 Kjaergaard, C. H. *et al.* Spectroscopic and computational insight into the activation of O-2 by the
694 mononuclear Cu center in Polysaccharide monoxygenases. *Abstr. Pap. Am. Chem. S.* **248**, (2014).
- 695 44 Lefort, V., Desper, R. & Gascuel, O. FastME 2.0: A Comprehensive, Accurate, and Fast Distance-
696 Based Phylogeny Inference Program. *Mol. Biol. Evol.* **32**, 2798-2800, (2015).
- 697 45 Goubet, F., Jackson, P., Deery, M. J. & Dupree, P. Polysaccharide analysis using carbohydrate gel
698 electrophoresis: A method to study plant cell wall polysaccharides and polysaccharide hydrolases.
699 *Anal. Biochem.* **300**, 53-68, (2002).
- 700 46 Tryfona, T. *et al.* Carbohydrate structural analysis of wheat flour arabinogalactan protein.
701 *Carbohydr. Res.* **345**, 2648-2656, (2010).
- 702 47 Rojas-Macias, M. A. & Lutteke, T. Statistical analysis of amino acids in the vicinity of carbohydrate
703 residues performed by GlyVicinity. *Methods Mol Biol* **1273**, 215-226, (2015).
- 704 48 Stoll, S. & Schweiger, A. EasySpin, a comprehensive software package for spectral simulation and
705 analysis in EPR. *J Magn Reson* **178**, 42-55, (2006).
- 706 49 MATLAB and Statistics Toolbox Release 2014a (The MathWorks, I., Natick, Massachusetts, United
707 States).

708

709 **Acknowledgements**

710 We wish to thank MAXLAB, Sweden and the European Synchrotron Radiation Facility
711 (ESRF), France, for synchrotron beamtime and assistance. Travel to synchrotrons was
712 supported by the Danish Ministry of Higher Education and Science through the Instrument
713 Center DANSCATT and the European Community's Seventh Framework Programme
714 (FP7/2007-2013) under BioStruct-X (grant agreement 283570).

715 This work was supported by the UK Biotechnology and Biological Sciences Research
716 Council (grant numbers BB/L000423/1 to P.D. and P.H.W., and BB/L021633/1 to P.H.W.)
717 and the Danish Council for Strategic Research (grant numbers 12-134923 to L.L.L. and
718 12-134922 to K.S.J.).

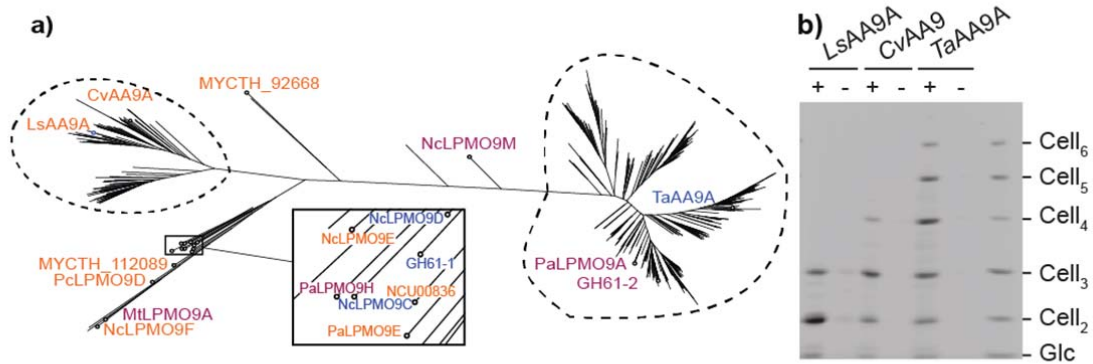
719 **Author contributions**

720 T.J.S. carried out most of the activity assays, assisted by T.T. and L.F.L.W. K.E.H.F.
721 carried out most of the structural studies with J.C.P., T.T. and L.L.L. L.C. carried out EPR
722 spectroscopy. L.N. and B.H. carried out phylogenetic studies. M.T. and K.S. carried out
723 target protein identification and production. P.D., L.L.L. and P.W. supervised the
724 experimental work. T.J.S., K.E.H.F., K.S.J.O., P.W., L.L.L. and P.D. analysed the data and
725 wrote the paper.

726 **Competing Financial Interests**

727 M.T. and K.S. are employees of Novozymes, a producer of enzymes for industrial use.
728

729



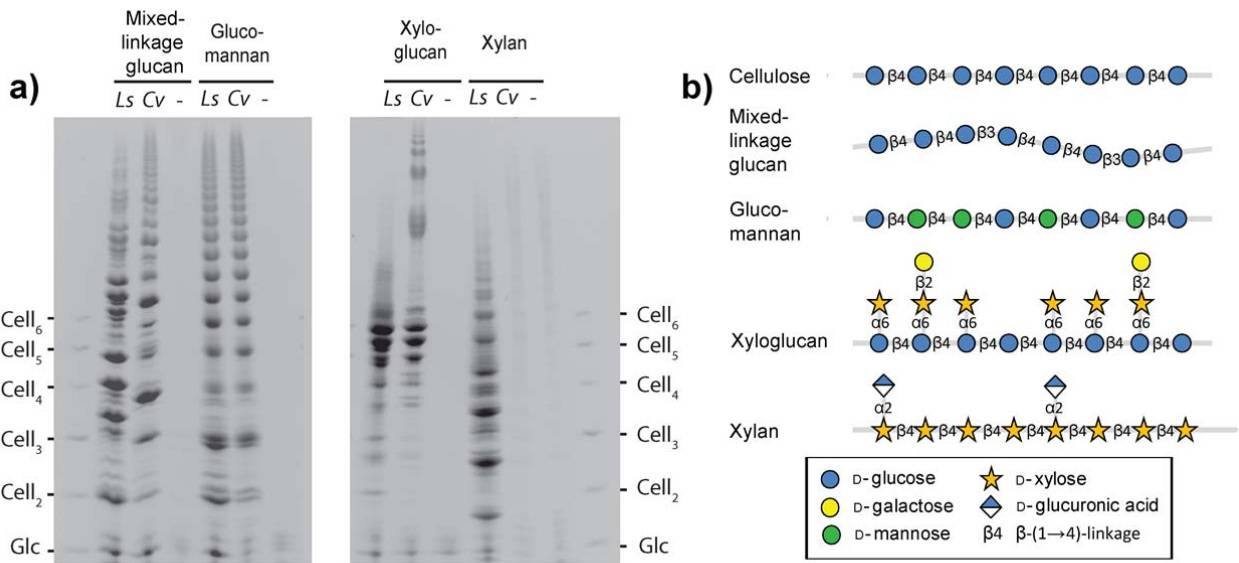
730

731

732

733 **Figure 1: Sequence similarity between *LsAA9A*, *CvAA9A* and *TaAA9A* and analysis**
734 **of their reaction products. a**, Distance tree of 444 selected AA9 sequences (see
735 methods). Blue, purple and orange labels designate AA9 enzymes that oxidize the sugar
736 ring at C1, C4 and C1+C4, respectively. See Supplementary Table 1 for protein accession
737 numbers. Unlabelled branches represent AA9 enzymes for which the regioselectivity of
738 oxidation is not available from the literature. **b**, PACE gel showing reaction products of the
739 three enzymes on PASC; +, incubation with 4mM ascorbate; -, incubation without
740 ascorbate (performed in triplicate).

741



742

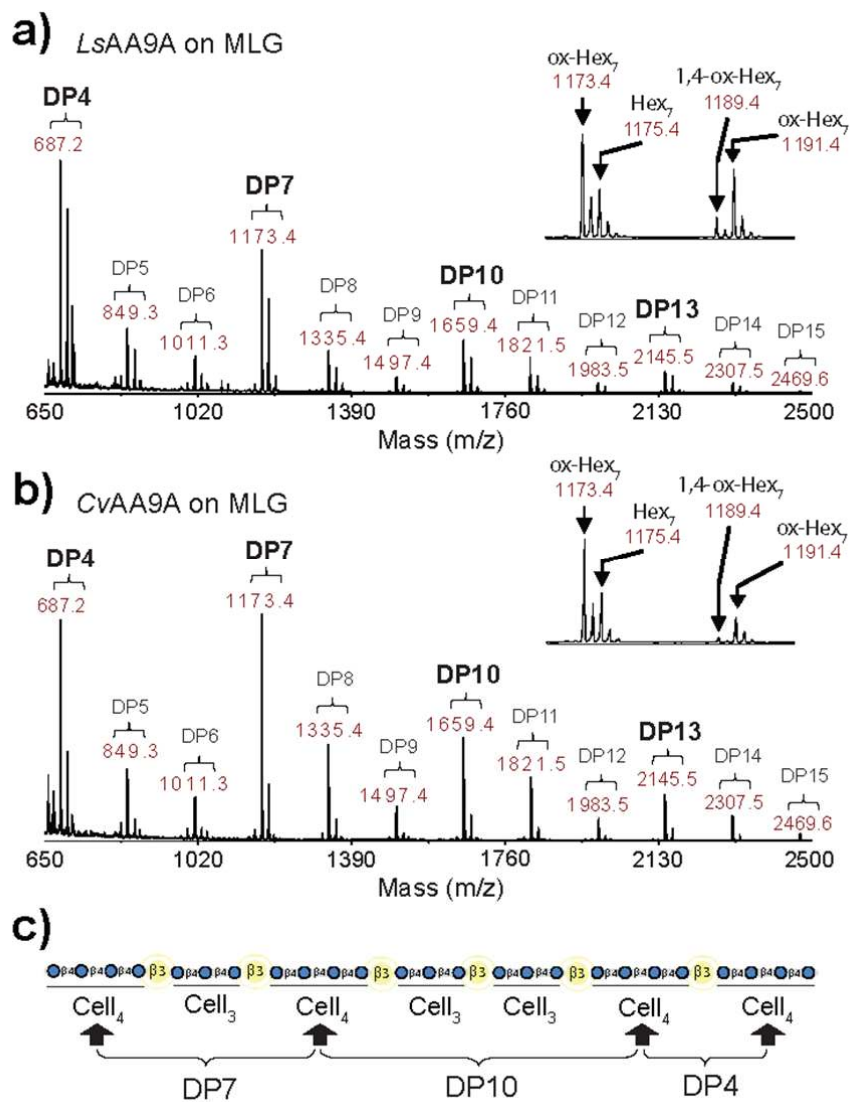
743 **Figure 2: Comparison of *LsAA9A* and *CvAA9A* action on non-cellulosic substrates.**

744 **a**, PACE gel showing digestion products on lignocellulosic polysaccharides with 4mM

745 ascorbate reducing agent. *Ls*, *LsAA9A*; *Cv*, *CvAA9A*; -, no enzyme. **b**, Structures of

746 polysaccharides.

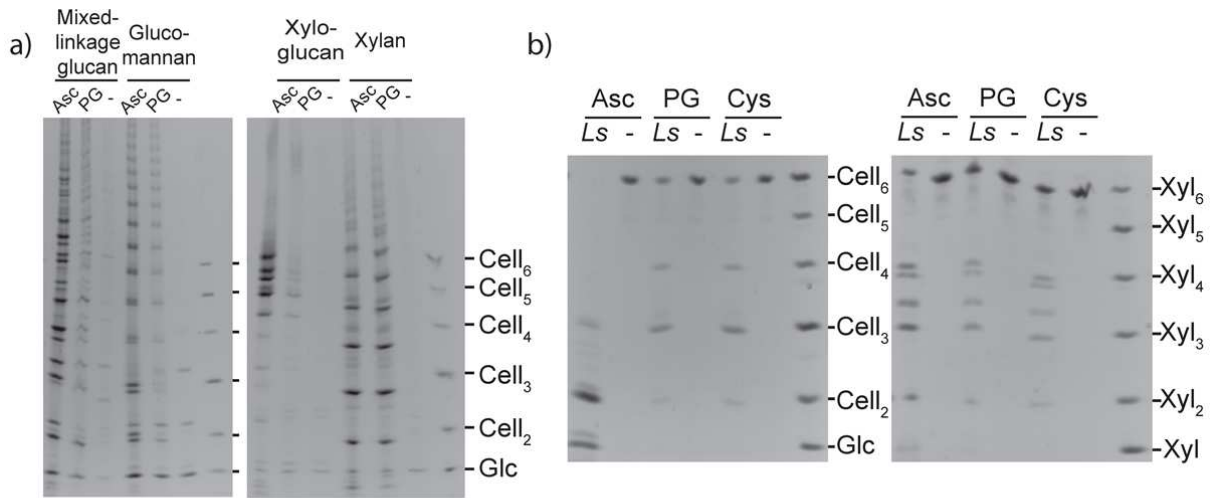
747



748

749 **Figure 3: LsAA9A and CvAA9A digestion products of MLG suggest preference for**
 750 **Cell₄ region cleavage.** Products of LsAA9A (a) and CvAA9A (b) activity on barley MLG
 751 with 4mM ascorbate were analysed by MALDI-ToF MS. Both enzymes can produce both
 752 C1 and C4 oxidation on MLG (1,4-ox; oxidized C1 and C4. See insets). Further,
 753 oligosaccharide profiles show a distinct pattern indicative of the mechanism of attack and
 754 substrate specificity of each enzyme on MLG. c, proposed region of cleavage.

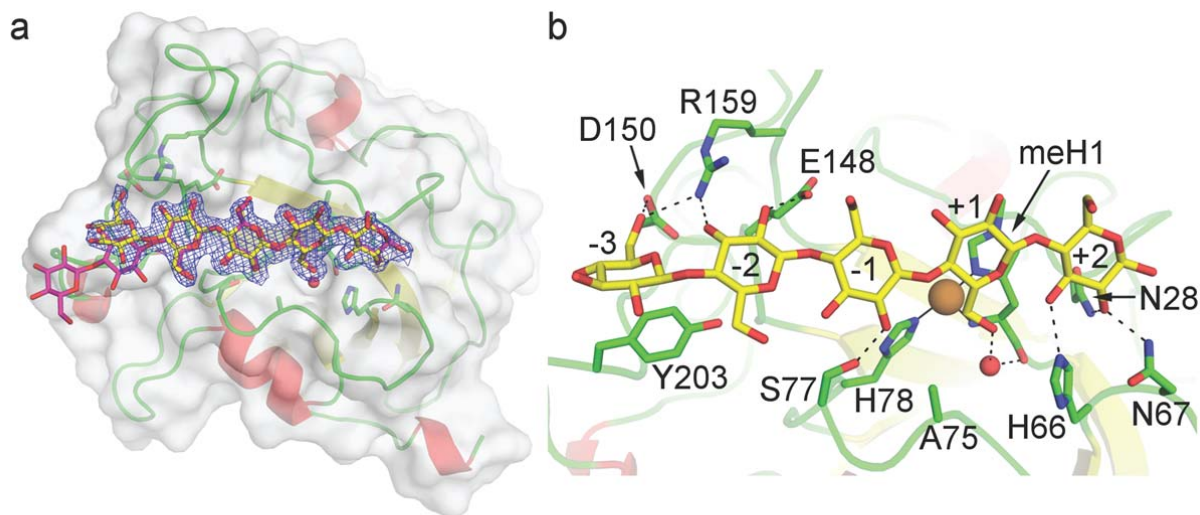
755



756

757 **Figure 4: *LsAA9A* activity on different poly- and oligosaccharide substrates show**
 758 **differing sensitivity to reducing agent potential.** a, PACE gels showing products of
 759 *LsAA9A* activity on MLG, glucomannan, xyloglucan and xylan polysaccharides using 4mM
 760 ascorbate or 4mM pyrogallol as reductants. The migration standards are cello
 761 oligosaccharides. b, PACE gels showing products of *LsAA9A* activity on Cell₆ and Xyl₆
 762 oligosaccharides using 4mM ascorbate, pyrogallol and cysteine as reductants. Asc,
 763 Ascorbate; PG, pyrogallol; Cys, cysteine.

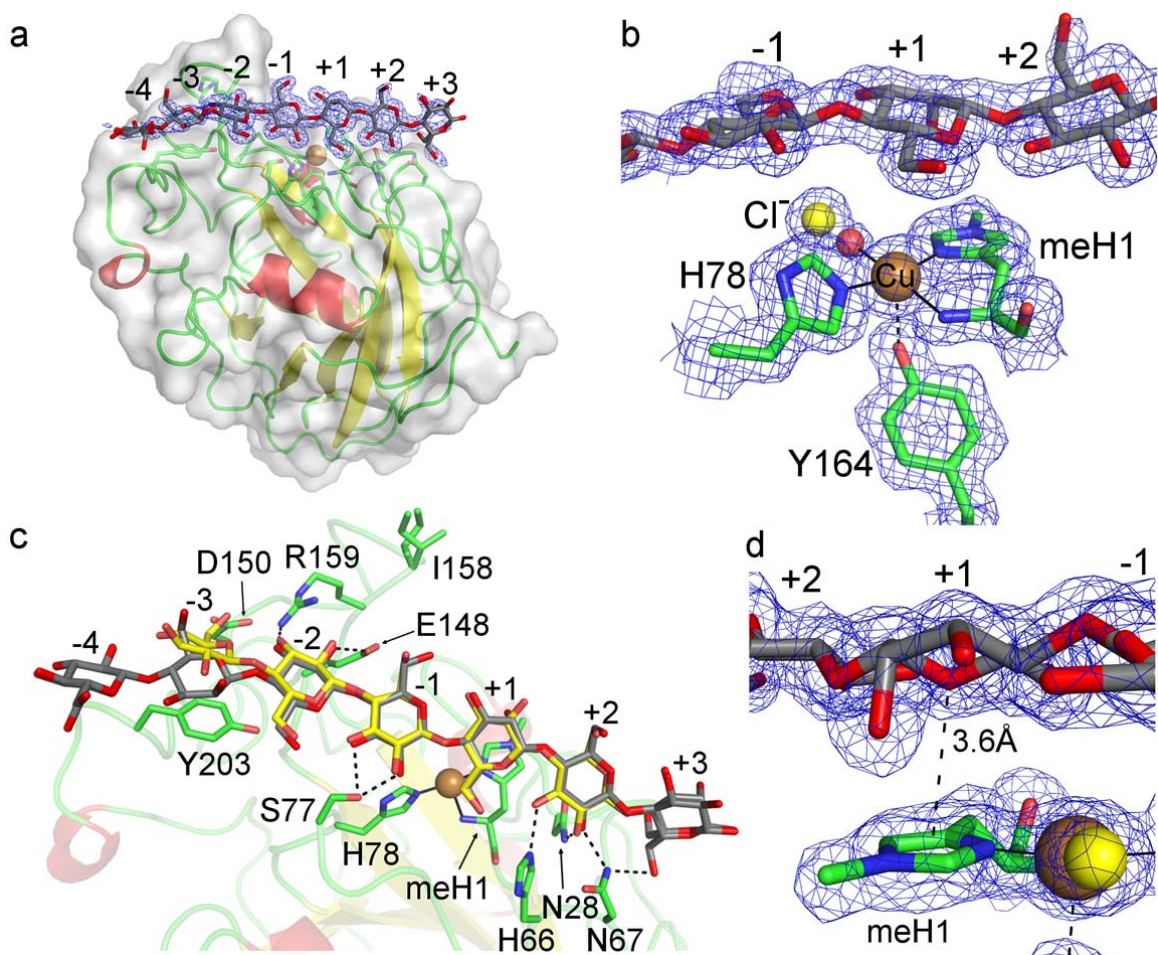
764



765

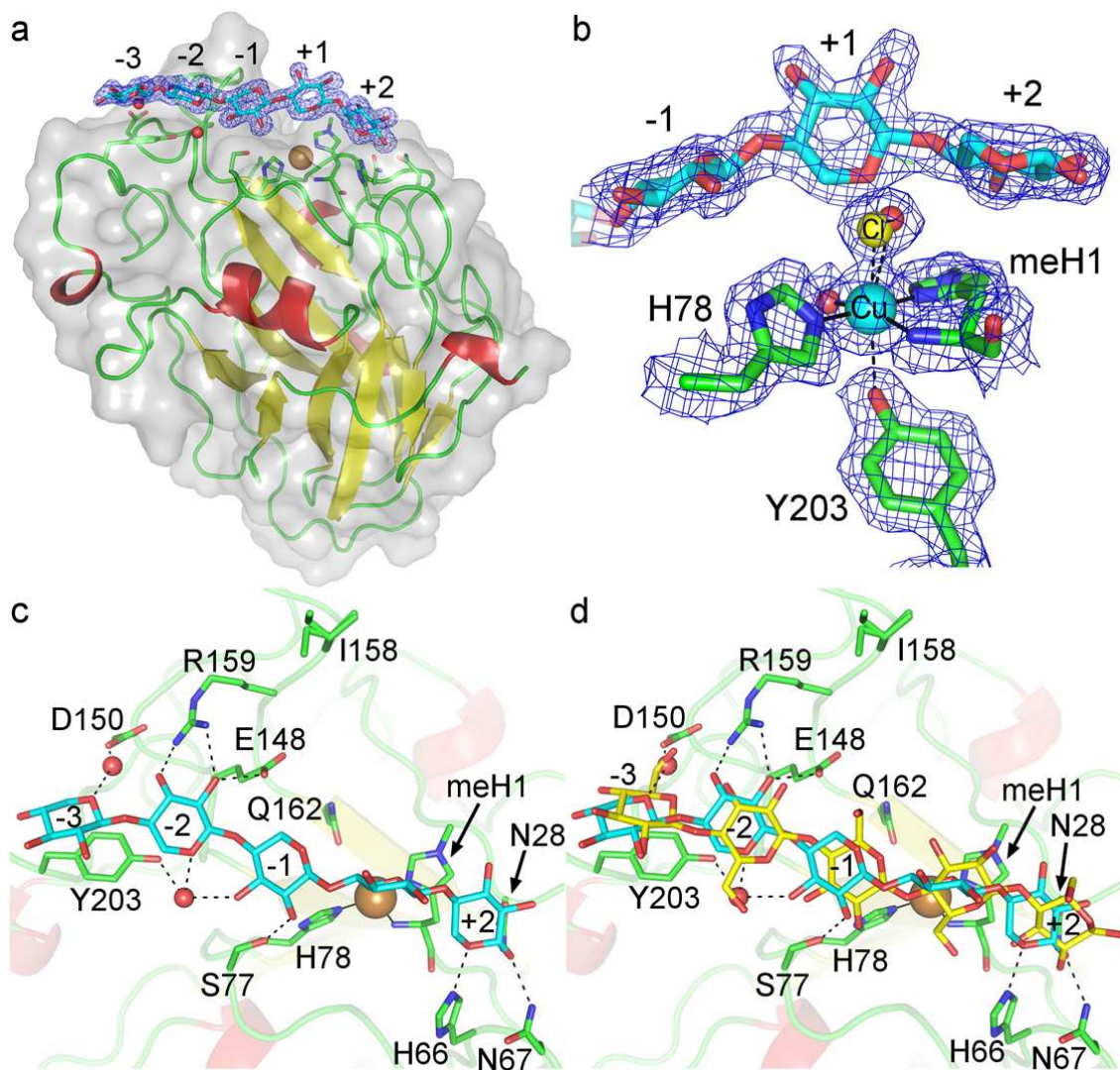
766 **Figure 5: *LsAA9A:Cell₅* structure shows interactions at subsites -3 to +2.** a, Cell₅
 767 (yellow) is well defined in subsites -3 to +2. A 2F_{obs}-F_{calc} electron density map is shown at
 768 1σ contour level. The structure shows no crystal contact induced distortion of the Cell₅
 769 substrate when compared to Cell₆ (magenta). b, *LsAA9A-Cell₅* interactions are shown as
 770 dashes. An additional interaction between subsite -3 (O)6 and Asp150 is gained in the
 771 absence of symmetry related contacts to the substrate.

772



773

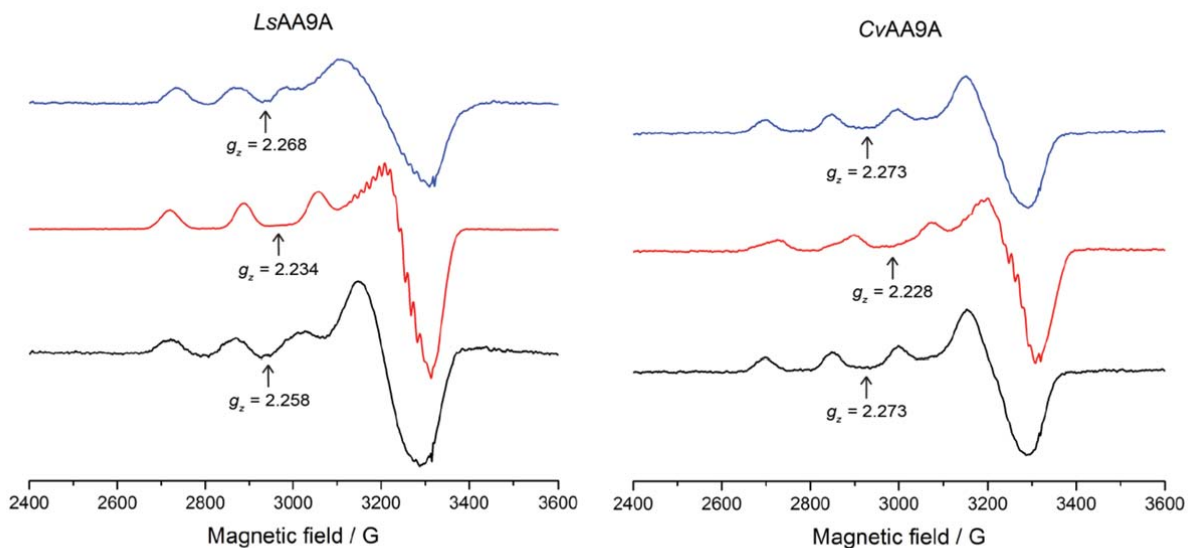
774 **Figure 6: Structure of the *LsAA9A*:glucomannan oligosaccharide complex.** **a,**
 775 Overall structure of *LsAA9A* with GM (blue) bound from subsite -4 to +3. **b,** Close up of the
 776 active site with GM fragment bound at subsite -1 to +2. Axial coordinations are in black
 777 dashes while equatorial coordinations are in full black lines. **c,** Top-down view of
 778 *LsAA9A*:GM (GM in grey) and for comparison *LsAA9A*:Cell₅ (Cell₅ in yellow). Dashed lines
 779 show interactions within hydrogen bond distance (2.8 Å). **d,** The C2-hydroxyl of mannose
 780 is clearly visible in the density at subsite +1. The pyranose O5-imidazole ring interaction
 781 (3.6 Å) is indicated with dashes. The interaction of MeHis and the mannosyl residue is
 782 very similar to the interaction with glucosyl residues in previous complexes³⁸. A $2F_{\text{obs}}-F_{\text{calc}}$
 783 electron density map is shown at 1σ contour level for panels a, b and d.



784

785 **Figure 7: Structure of the *LsAA9A*:xylo-oligosaccharide complex.** **a**, *LsAA9A*:Xyl₅ with
 786 bound substrate (in cyan) from subsite -3 to +2. **b**, Active site structure in the low dose
 787 *LsAA9A*:Xyl₅ structure, showing that the +1 xylosyl unit does not direct interact with the
 788 enzyme or displace the axial ligand on the copper (modelled as chloride and water in
 789 0.5:0.5 ratio). **c**, Top-down view *LsAA9A*:Xyl₅ (in cyan). **d**, Top-down view *LsAA9A*:Xyl₅ (in
 790 cyan) and *LsAA9A*:Cell₅ (in yellow) shown for comparison. A $2F_{\text{obs}}-F_{\text{calc}}$ electron density
 791 map is shown at 1σ contour level in panels a and b.

792



793

794 **Figure 8: X band cw EPR spectra of LsAA9A (left) and CvAA9A (right), 150 K.**
 795 Spectra were collected in the presence of 1 M NaCl (black), Cell₆ and 200 mM NaCl (red),
 796 or Xyl₆ and 1 M NaCl (blue).

797

Polysaccharide	LsAA9A		CvAA9	
	Activity	Notes	Activity	Notes
Cellulose and cello-oligosaccharides	++	Activity on both cellulose oligosaccharides and insoluble cellulose material (PASC).	++	Activity on both cellulose oligosaccharides and insoluble cellulose material (PASC).
MLG	++	Pattern suggests β -(1→3)-bonds accommodated at specific places within active site, but not between -1 and +1.	++	Pattern suggests β -(1→3)-bonds accommodated at specific places within active site, but not between -1 and +1.
Glucomannan and Man ₆	++	Cleavage can occur with Glc or mannose at -1 or +1. Inactivity on Man ₆ indicates some Glc C2 hydroxyl orientation needs to be present between -3 and +3.	++	Cleavage can occur with Glc or mannose at -1 or +1. Inactivity on Man ₆ indicates some Glc C2 hydroxyl orientation needs to be present between -3 and +3.
Xyloglucan	++	Cleavage occurs with unsubstituted Glc at subsite +1. Xylosyl substitution at -3, -2, -1, +2 and +3. Galactosyl-xylosyl substitutions can occur at either -2, -1 and/or +3.	++	Cleavage occurs with unsubstituted Glc at subsite +1. Xylosyl substitution at -3, -2, -1, +2 and +3. Galactosyl-xylosyl substitutions can occur at either -2, -1 and/or +3.
Xylan and Xyl ₆	+	Activity on both. Weak Xyl ₆ activity compared to Cell ₆ suggests that, while Glc C6 is not required for activity, it is very important at certain sites, such as +1.	+/-	Much poorer activity of CvAA9A compared with LsAA9A.
Starch	-	Absence of activity indicates that LsAA9A necessarily cleaves β -(1→4)-bonds.	-	Absence of activity indicates that CvAA9A necessarily cleaves β -(1→4)-bonds.
Laminarin	-		-	
G4G3G4G (MLG oligosaccharide)	-		-	
Chitin	-	Absence of activity indicates that LsAA9A either requires O2 interactions or cannot accommodate N-Acetyl on amino C2.	-	Absence of activity indicates that CvAA9A either requires O2 interactions or cannot accommodate N-Acetyl on amino C2.

798 **Table 1: Summary of activity assays on different substrates.** Semi-quantitative activity
799 results summarising the activity of *LsAA9A* and *CvAA9A* on the range of different
800 substrates used in this manuscript.

801

Enzyme-substrate combination	g_z	A_z (MHz)	Comments
No NaCl			
<i>LsAA9A</i> -H ₂ O	2.279	458	Weak superhyperfine (SHF) coupling
<i>LsAA9A</i> +Cell ₆	2.273	515	Intense SHF coupling
<i>LsAA9A</i> +avicel	2.278	470	Weak SHF coupling
<i>LsAA9A</i> +xylan	2.272	480	Spectrum complicated by organic-based radicals in perpendicular region
<i>LsAA9A</i> +glucomannan	2.232	518	Very likely NaCl contamination in the substrate. Intense SHF coupling
<i>LsAA9A</i> +xyloglucan	2.270	515	Very intense SHF coupling.
200 mM NaCl			
<i>LsAA9A</i> -Cl	2.258	455	Likely mixture of H ₂ O and Cl species.
<i>LsAA9A</i> +Cell ₆	2.234	517	Intense SHF coupling
<i>LsAA9A</i> +avicel	2.232	522	Slight change in perpendicular region, some appearance of SHF coupling
<i>LsAA9A</i> +xylan	2.270	470	Spectrum complicated by organic-based radicals in perpendicular region
<i>LsAA9A</i> +solubilised xylan	2.272	470	radical impurities present in the perpendicular region
<i>LsAA9A</i> +glucomannan	2.231	520	Intense SHF coupling
<i>LsAA9A</i> +solubilised glucomannan	2.233	515	Intense SHF coupling
<i>LsAA9A</i> +xyloglucan	2.228	530	Intense SHF coupling
<i>LsAA9A</i> +Xyl ₆	2.268	400	Very rhombic, different from both Cell ₆ -bound and unbound protein, intense SHF coupling. Could only be achieved with very high Xyl ₆ concentrations.
<i>CvAA9A</i>	2.273	476	Likely no Cl species present
<i>CvAA9A</i> +Cell ₆	2.228	527	Mixture of C ₆ -bound and unbound <i>CvAA9A</i> . Some SHF coupling visible. Full binding could not be achieved even with large excess of Cell ₆
<i>CvAA9A</i> -1 M NaCl	2.273	468	Likely no Cl species present even in the presence of 1 M NaCl
<i>CvAA9A</i> +Xyl ₆ -1 M NaCl	2.273	468	Spectrum identical to the unbound form, even at very high Xyl ₆ concentrations.

802 **Table 2: Spin-Hamiltonian parameters (parallel region) for *LsAA9A* and *CvAA9A* in**
803 **contact with substrates.** The experiments were performed with or without 0.2 M chloride.
804 For xylohexaose 1.0 M chloride was used. Spectra are shown in Supplementary Fig. 12–
805 13.

806